A Long-Range Surface Plasmon Resonance/Probe/Silver Nanoparticle (LRSPR-P-NP) Nanoantenna Configuration for Surface-Enhanced Raman Scattering

ARTICLE *in* JOURNAL OF PHYSICAL CHEMISTRY LETTERS · SEPTEMBER 2012

Impact Factor: 7.46 · DOI: 10.1021/jz300948t

6 AUTHORS, INCLUDING:

Shuping Xu
Jilin University
100 PUBLICATIONS **1,370** CITATIONS
SEE PROFILE

Haibo Li
Jilin University
36 PUBLICATIONS **645** CITATIONS
SEE PROFILE

THE JOURNAL OF PHYSICAL CHEMISTRY Letters

Letter

pubs.acs.org/JPCL

A Long-Range Surface Plasmon Resonance/Probe/Silver Nanoparticle (LRSPR-P-NP) Nanoantenna Configuration for Surface-Enhanced Raman Scattering

Xuyang Xuan,[†] Shuping Xu,[†] Yu Liu,[‡] Haibo Li,[†] Weiqing Xu,*[,†] and John R. Lombardi[§]

[†]State Key Laboratory of Supramolecular Structure and Materials, Jilin University, Changchun, 130012, People's Republic of China

[‡]State Key Laboratory of Applied Optics, Changchun Institute of Optics, Fine Mechanics and Physics, Chinese Academy of Sciences, Changchun, 130033, People's Republic of China

[§]Department of Chemistry, City College of New York, New York 10031, United States

Supporting Information

ABSTRACT: The purpose of this paper is to enhance Raman signals with a plasmonic nanoantenna based on a long-range surface plasmon resonance/probe/silver nanoparticle (LRSPR-P-NP) sandwich configuration. The finite-difference time-domain simulation shows that the electromagnetic field at the gap between the silver film and a silver nanoparticle increases by a factor of about 2.1×10^4. The resonance condition of this plasmonic nanoantenna was optimized by incident angle-dependent surface-enhanced Raman scattering (SERS) spectroscopy under an evanescent field excitation mode. The SERS signal obtained under the LRSPR-P-NP configuration at the LRSPR angle was 40 times higher than that collected on the planar film plasmonic nanoantenna. The enhancement factor of the LRSPR-P-NP configuration was 9.2×10^8. This plasmonic nanoantenna was also applied for pH sensing.

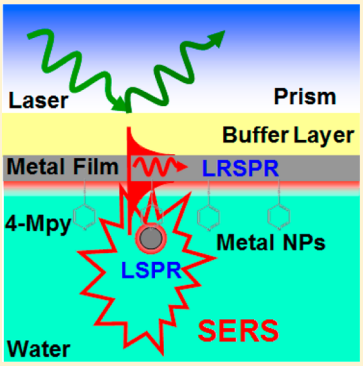

SECTION: Plasmonics, Optical Materials, and Hard Matter

Radio and microwave antennas are predominantly used to control and guide electromagnetic field at radio and microwave frequencies. In direct analogy to the function of radio antennas,[1−5] nanoantennas act as a bridge of the optical far field and near field. During the energy transfer process, nanoantennas enable an efficient transfer of electromagnetic energy from near to far field.[6] Plasmonic nanoantennas exploit the unique properties of metal nanostructures.[7] They represented the forms of the strongly coupled plasmons at optical frequencies. Plasmonic nanoantennas can absorb and focus incident light into a subdiffraction limited volume, and can also efficiently couple out stored energy, acting now as emitting antennas. These pave the way to manipulate, control, and visualize optical field on the nanometer scale.[8−10] Also, they widen the applications of plasmonic materials in the field of surface-enhanced fluorescence,[11−13] plasmonic solar cells,[14−16] nanomedicine,[17−21] and sensing.[22,23]

To design and construct a plasmonic antenna for stronger electromagnetic coupling is an objective that has been pursued by scientists.[24−26] A great number of plasmonic antennas were fabricated by physical micromachining methods and their abilities for light manipulation were discussed in nanometer scale. Pakizeh et al.[27] reported an ultracompact plasmonic nanoantenna built up by two gold disks. They found a forward−backward directionality as high as 18 dB at 665 nm that closely matched the antiphase plasmon resonance of the hybridized nanoparticle (NP) system. This unique unidirectionality concept paves the way for nano- and biophotonics applications of nanoantenna. Moreover, a high directivity antenna named the Yagi-Uda antenna was designed, which basically consisted of a one-dimensional array of antenna elements. This nano-optical antenna array is an efficient tool for the spatial control of light emission in guiding the absorption and emission of light.[28] Altug et al.[29] demonstrated a compact multiresonant metamaterial structure based on the integrated U- and T-shaped nanoaperture antennas. The resonant modes were easily tuned to the desired frequencies by simply changing the structural parameters of the apertures, and the near field enhancement was over 1200-fold larger for the first and second modes. Besides these, the reported plasmonic antennas involved a metallic "bowtie" structure consisting of two opposing tip-to-tip Au triangles,[30] dolmen-type resonators,[31] gold NP trimers,[32] silver NP dimers,[33] flowers,[34] nanostars,[35] gold rings,[36] and so on.

The use of plasmonic nanoantennas for plasmonic-enhanced spectroscopy has attracted many researchers in recent years.[37] It was reported that the nanoantenna composed by relatively dense corrugated nanowires exhibited relatively higher reproducibility and surface-enhanced Raman scattering

Received: July 14, 2012
Accepted: September 12, 2012

   dx.doi.org/10.1021/jz300948t | J. Phys. Chem. Lett. 2012, 3, 2773−2778

(SERS) enhancement.[38] Chou et al. proposed a new SERS substrate that couples a dense three-dimensional (3-D) cavity nanoantenna array, which led to the achievement of an area-average SERS enhancement of 1.2×10^9 and large-area uniformity with the variation of less than 25%.[39] Zhang et al. described plasmonic interactions in a suspended gold bowtie nanoantenna, in which the SERS enhancement factor (EF) exceeded 10^{11} at the gap of two bowties.[40] Recently, a planar-film plasmonic antenna excited in attenuated total reflectance mode was reported by our group.[41] A prism-type surface plasmon resonance (SPR) configuration was used to couple the surface plasmons for SERS excitation and collection. The results showed that this planar-film plasmonic antenna was able to increase the collection efficiency with a good emission directivity in space (divergence angle < 3°).[41]

In this paper, we propose a plasmonic nanoantenna based on a long-range surface plasmon resonance/probe/silver nanoparticle (LRSPR-P-NP) sandwich configuration for SERS study. We employed the incident angle-dependent spectroscopy to optimize the coupling efficiency of this plasmonic nanoantenna. The electromagnetic field in the gap between metal film and metal NPs was simulated by the finite-difference time-domain (FDTD) method. This LRSPR-P-NP antenna not only supports a high SERS signal, but also provides the structural changes of analytes. In addition, we are able to use this LRSPR-P-NP configuration for pH sensing.

The Design of the LRSPR-P-NP Antenna. Scheme 1 shows the designed plasmonic nanoantenna that we used to detect SERS spectra of 4-mercaptopyridine (4-Mpy). Differing from the antennas that have been reported,[26−29] this new plasmonic nanoantenna was excited in the evanescent field due to its prism-typed SPR configuration, which could reduce the background of SERS spectra from Rayleigh scattering.

Scheme 1. The Setup of the LRSPR-P-NP Plasmonic Nanoantenna for SERS

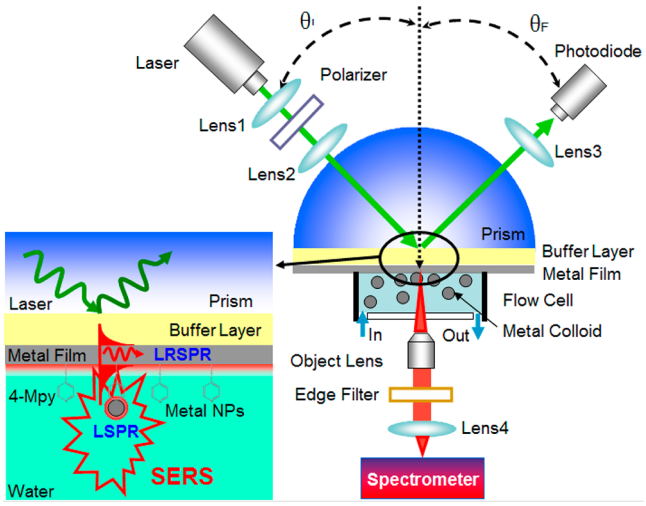

The design of this new plasmonic nanoantenna is different from the previous study. It is considered from two key points, namely, the manipulation of two coupling processes from the far to near fields and the near to far fields. In the present study, the photonic energy in the far field converting to the near-field energy was completed by a LRSPR configuration, which is a light-harvesting process. When the incident light propagated to the metal film layer that was embedded in two dielectric layers, the LRSPs emerged. Owing to the existence of an MgF_2 buffer layer, the LRSPRs possess longer surface propagation lengths, higher surface electric field strengths, narrower angular resonance curves, and lower resonance angle compared with the conventional SPs.[42−47] These advantages of LRSPRs will greatly facilitate light harvesting, further improving the excitation of probes. In the next process, the LRSPs at the Raman-shift frequency selectively coupled with metal NPs. The localized surface plasmons of metal NPs, which are the conduction electrons of NPs in collective oscillations, led to strong radiation in far field. Since a lot of nanogaps between the metal film and metal particles were formed, which were known as "hot spots", great strong local electromagnetic fields located at the gaps will be expected. These can inject the excitation of probes in the vicinity of gaps, generating stronger SERS by means of localized surface plasmons. Differing from the previous study of the gap-enhanced SERS, metal NPs are not just simply used to enhance SERS signals. In this nanoantenna structure, metal NPs not only take the role of transferring energy from near to far fields, but also increase the scattering cross section relative to Raman probe molecules for stronger radiation in far field.

Optimization of the Resonance Condition of the LRSPR-P-NP Antenna. In order to obtain a better coupling effect, we optimized the incidence angle on the LRSPR-P-NP configuration to achieve resonance. We measured the angle-dependent SERS spectra by using a self-developed SPR-SERS spectrometer.[48] More details about this setup and how it works are provided in the Supporting Information. Figure 1A,B shows the incident angle-dependent SERS spectra of 4-Mpy on a LRSPR planar-film nanoantenna and a LRSPR-P-NP nanoantenna. Figure 1C shows the SPR curves and the plots of SERS intensities at 1096 and 1092 cm^{-1} with the incidence angles on the planar film nanoantenna and LRSPR-P-NP nanoantenna. The resonance angle of 4-Mpy on the planar film nanoantenna is 64.78°, and the incident angle at maximal SERS intensity is 64.70°(a and c in Figure 1C). The SERS signal in the resonance condition (64.70°) is about 32 times than that at nonresonance angles (e.g., 62°). Figure 1C(b) shows the SPR curve of 4-Mpy on the LRSPR-P-NP nanoantenna. The resonance angle of LRSPR in Figure 1C(b) (64.64°) has a 0.24° decrease compared with that in Figure 1C(a). The change of SPR angle reflects the fact that the silver NPs were successfully assembled on the silver film through 4-Mpy. In addition, the strongest SERS intensity on the LRSPR-P-NP nanoantenna was obtained when the incident angle was 64.40° (d in Figure 1C), which presents a cocontribution for SERS from both the LRSPR and localized SPR.

Electric Field Distribution on the LRSPR-P-NP Nanoantenna. The high SERS signal is considered to derive from the effective electric field coupling of silver NPs with the silver film. In previous work, simulation results show that the electric field at the gap between a silver film and a silver NP in a conventional SPR configuration increased by a factor of about 4000, and experimental results showed that the SERS signal under the silver NPs assisted localized surface plasmon and propagating surface plasmon (LSP-PSP) coenhancement was more than 50 times higher than the signal obtained on the vacuum-deposited silver film.[49] These are in good agreement with our results. Figure 2 shows the simulation results of electric field distribution of the LRSPR-P-NP configuration (Lumerical FDTD Solutions software, Canada). More details about the FDTD are provided in Supporting Information. The electric

dx.doi.org/10.1021/jz300948t | J. Phys. Chem. Lett. 2012, 3, 2773−2778

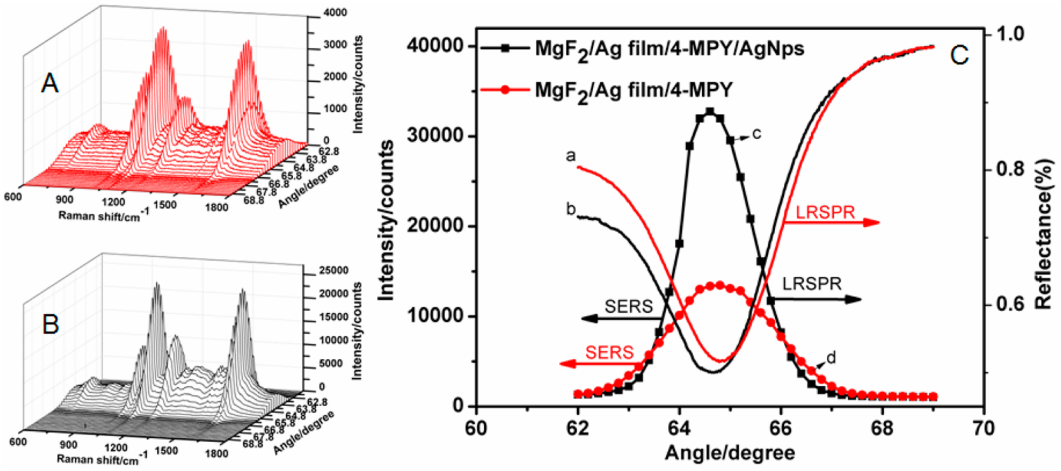

Figure 1. (A) The incident angle-dependent SERS spectra of 4-Mpy on a planar-film SERS antenna without silver NPs. The integration time was 3 s. (B) The incident angle-dependent SERS spectra of 4-Mpy on a LRSPR-P-NP configuration. The integration time was 1 s. Curves a and b in panel C are the SPR curves of the planar-film SERS antenna and the LRSPR-P-NP configuration. Curves c and d in panel C are the SERS intensity profiles of the incident angle-dependent SERS of 4-Mpy on planar-film SERS antenna and the LRSPR-P-NP configuration. The SERS intensity profile for curve c was obtained by plotting the SERS band at 1096 cm^{-1} in panel A while the 1092 cm^{-1} band in panel B was chosen for plotting curve d.

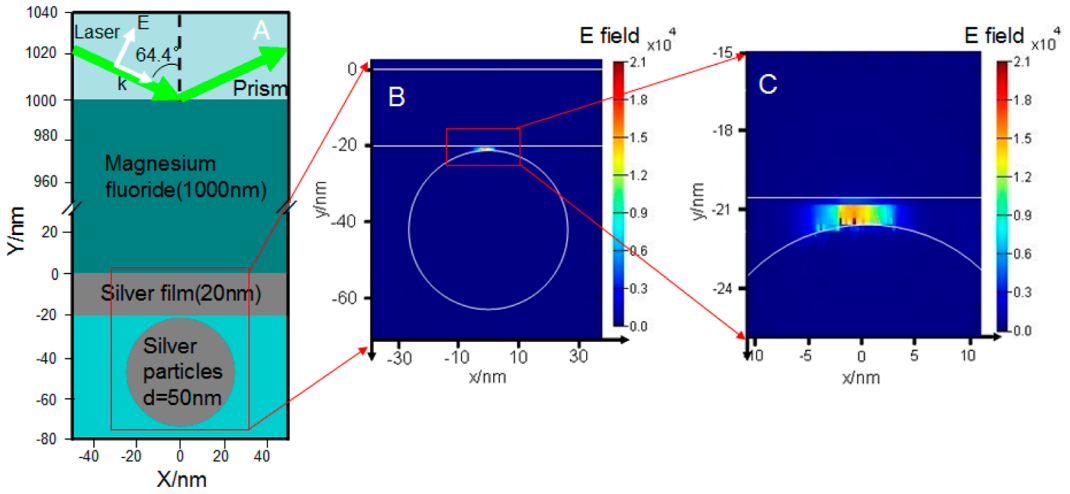

Figure 2. (a) Schematic diagram of the LRSPR-P-NP configuration used for FDTD simulation. A 1 nm gap is set between the silver film and silver NPs. k and E indicate the wave vector and electric vector of the incident light. The dielectric surrounding around the silver NP and silver film is water. (b) FDTD simulation of the electric field distribution for the LRSPR-P-NP system. (c) Magnification of the E field distribution at the vicinity of the gap.

field at the gap between the silver film and a silver NP increases by a factor of about 2.1×10^4, which proves that stronger SERS was caused by the electromagnetic enhancement. Moreover, it is noted that the electric field at the gap in the LRSPR-P-NP configuration is 3 times of that at the gap in the conventional SPR configuration, which indicates the LRSPR works better for light harvesting than the conventional SPR.

Spectral Analysis. Figure 3A(a) shows the SERS spectrum of 4-Mpy after they were absorbed on the silver film. Compared with the Raman spectrum of 4-Mpy (Figure S1 in Supporting Information), a strong peak at 713 cm^{-1} (β(CC)/γ(C−S)) in Figure S1 shows a remarkable downward shift to a weak peak at 709 cm^{-1} (curve b).[50,51] Also, the band at 1100 cm^{-1} was dramatically enhanced upon the adsorption. These changes can be explained by the formation of a S−Ag band after the 4-Mpy was absorbed on the silver surface.

Figure 3A(b) shows the SERS spectrum of 4-Mpy after silver NPs were assembled. The changes in SERS intensities in Figure 3A(a),(b) were also analyzed, which reflect the changes in 4-Mpy before and after the assembly of silver NPs. First, the SERS intensity at 1092 cm^{-1} in Figure 3A(b) has 40 times enhancement relative to that in (a). This is caused by the strong electric field at the gaps between silver NPs and silver film. Second, in Figure 3A(a), the intensity ratio of 1606 cm^{-1}/1575 cm^{-1} is relatively low, while it increases in Figure 3A(b). At the same time, a new peak at 1206 cm^{-1} appears while the peak at 1221 cm^{-1} disappears. This is because of the protonation effect on the N atom of the pyridine ring with the pH value in solution.[51] To further prove this, the bands at 1206 and 1221 cm^{-1} were resolved using a curvefit treatment. The result of band separation in Figure 3B,C agrees with our supposition that two bands overlap. We expect that these pH-sensitive bands can be applied for a SERS pH sensor (see Supporting Information).

Calculation of the EF of 4-Mpy in the LRSPR-P-NP Configuration. Here, we adopted the estimation of the average

dx.doi.org/10.1021/jz300948t | J. Phys. Chem. Lett. 2012, 3, 2773−2778

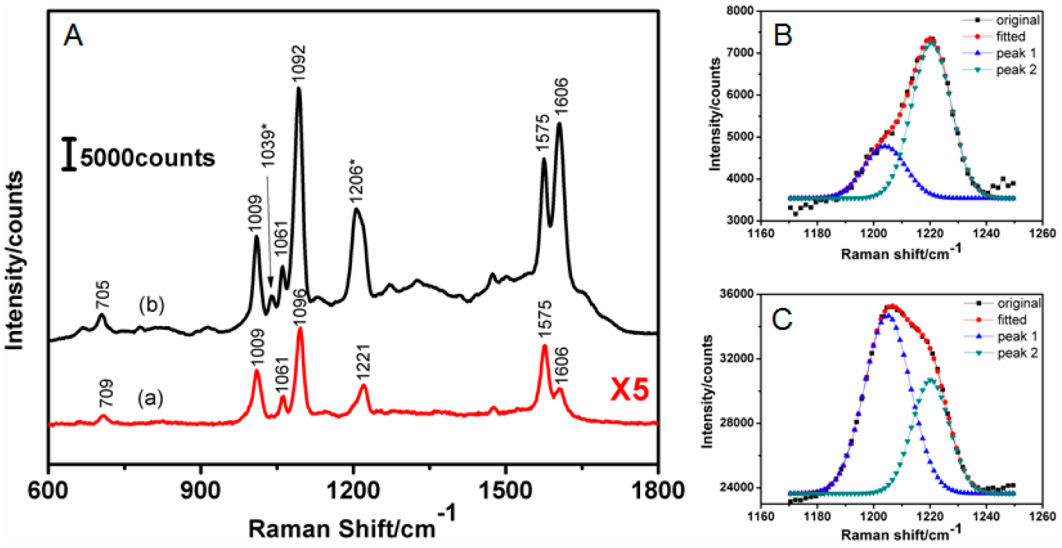

Figure 3. (A): (a) A SERS spectrum of 4-Mpy assembled on the Ag film. The resonance angle was located at 64.7°. The integration time was 3s. (b) A SERS spectrum of 4-Mpy obtained on the LRSPR-P-NP configuration under the resonance angle excitation (64.4°). The integration time was 1 s. Panels B and C show the peak separation of spectra (a) and (b) on the bands of 1206 and 1221 cm^{-1}.

SERS EF (G). More details about the calculation of G are stated in the Supporting Information. In this LRSPR-P-NP configuration, the value of G was calculated as 5.62 ($\pm$0.55) $\times$ 10^7.

For the LRSPR configuration in our previous work, G was calculated as 2.0 $\times$ 10^7.[52] It seems that not too much increase (only 2.8 times) in the LRSPR-P-NP configuration was observed relative to the LRSPR configuration. However, it should be noted that the G represents an average EF. If we consider the loading of silver NPs, which supports the LRSPR-P-NP configuration, the G will be different. The loading of silver NPs obtained from the AFM image in Figure S4B was 4%. The average G (5.62 $\times$ 10^7) contains a 4% contribution from the LRSPR-P-NP configuration and 96% contribution from individual LRSPR (in which G is 2.0 $\times$ 10^7). So, the modified G from the LRSPR-P-NP configuration was calculated as high as 9.2($\pm$1.4) $\times$ 10^8, which is comparable to the SERS enhancement level of "hottest sites"(the G is larger than 10^9).[53]

In summary, we designed a plasmonic nanoantenna based on a LRSPR-P-NP configuration for SERS detections and pH sensing. This SERS antenna was excited in evanescent field. The design of the LRSPR for light harvesting worked well for SERS excitation. The maximal SERS signal excited by the LRSPR-P-NP configuration was about 40 times stronger than that obtained on the planar film plasmonic nanoantenna. The maximal coupling efficiency was optimized around the resonance angles. According to the simulated results of FDTD, the electric field at the gap between the silver film and a silver NP increased by a factor of about 2.1 $\times$ 10^4. The modified EF of the LRSPR-P-NP configuration was obtained as high as 9.2($\pm$1.4) $\times$ 10^8. The protonation effect on 4-Mpy was used as a pH sensor. This novel plasmonic antenna has broad application prospects in plasmonic devices based on highly efficient light harvesting and radiation.

EXPERIMENTAL METHODS

Preparation of the LRSPR-P-NP Configuration. A LRSPR configuration was built first. On a K9 prism (the refractive index is 1.52 at 532 nm), a 1000 nm buffer layer (MgF_2, the refractive index is 1.38 at 532 nm) and a 20 nm silver film were successively deposited on it by the vacuum evaporation deposition method (the deposition rate was 0.2 nm/s). The thickness of deposited layers was measured by a surface profiler (Dektak 150, Veeco Co.). The penetration depth is calculated as 613 nm (see Supporting Information). After that, a layer of 4-mercaptopyridine (4-Mpy, 97%, Sigma Co.) was assembled on the silver surface by exposing the silver film in a 4-Mpy aqueous solution (1.0 $\times$ 10^{-5} M) for 20 min. Finally, silver NPs were linked by 4-Mpy as the final layer. It was completed by immersing the 4-Mpy modified LRSPR configuration in a silver colloid for 20 min. The silver colloid was prepared by Lee's method,[54] and the particle concentration was 2.48 $\times$ 10^{-11} M. The morphologies of the deposited silver film before and after the assembly of silver NPs were characterized by atomic force microscopy (AFM).

ASSOCIATED CONTENT

Supporting Information

(1) Configuration of the SPR-SERS microspectrometer, (2) the details of FDTD simulation, (3) theoretical calculation of the penetration depth, (4) the assignment of the Raman spectrum of 4-Mpy, (5) pH sensing, (6) AFM images of the deposited silver film before and after the assembly of silver NPs, and (7) calculation of the average EF (G), are included. These materials are available free of charge via the Internet at http://pubs.acs.org.

AUTHOR INFORMATION

Corresponding Author

*E-mail: xuwq@jlu.edu.cn.

Notes

The authors declare no competing financial interest.

ACKNOWLEDGMENTS

This work was supported by the National Natural Science Foundation of China (NSFC), Grant Nos. 20903043, 20973075, 21073073, and 91027010; the Research Fund for the Doctoral Program of Higher Education of China, Grant No. 20090061120089; and the National Instrumentation Program

(NIP) of the Ministry of Science and Technology of China No. 2011YQ03012408.

REFERENCES

(1) Kuhn, S.; Hakanson, U.; Rogobete, L.; Sandoghdar, V. Enhancement of Single-Molecule Fluorescence Using a Gold Nanoparticle as an Optical Nanoantenna. *Phys. Rev. Lett.* **2006**, *97*, 017402−017405.

(2) Muskens, O. L.; Giannini, V.; Sanchez-Gil, J. A.; Gomez-Rivas, J. Strong Enhancement of the Radiative Decay Rate of Emitters by Single Plasmonic Nanoantennas. *Nano Lett.* **2007**, *7*, 2871−2875.

(3) Taminiau, T. H.; Moerland, R. J.; Segerink, F. B.; Kuipers, L.; Van Hulst, N. F. $\lambda/4$ Resonance of an Optical Monopole Antenna Probed by Single Molecule Fluorescence. *Nano Lett.* **2007**, *7*, 28−33.

(4) Taminiau, T. H.; Stefani, F. D.; Segerink, F. B.; Van Hulst, N. F. Optical Antennas Direct Single-Molecule Emission. *Nat. Photonics* **2008**, *2*, 234−237.

(5) Greffet, J. -J. Nanoantennas for Light Emission. *Science* **2005**, *308*, 1561−1563.

(6) Giannini, V.; Fernández-Domínguez, A. I.; Heck, S. C.; Maier, S. A. Plasmonic Nanoantennas: Fundamentals and Their Use in Controlling the Radiative Properties of Nanoemitters. *Chem. Rev.* **2011**, *111*, 3888−3912.

(7) Taminiau, T. H.; Stefani, F. D.; Van Hulst, N. F. Single Emitters Coupled to Plasmonic Nano-antennas: Angular Emission and Collection Efficiency. *New J. Phys.* **2008**, *10*, 105005−105020.

(8) Ding, W.; Bachelot, R.; Kostcheev, S.; Royer, P.; De Lamaestre, R. E. Surface Plasmon Resonances in Silver Bowtie Nanoantennas with Varied Bow Angles. *J. Appl. Phys.* **2010**, *108*, 124314−124319.

(9) Verellen, N.; Sonnefraud, Y.; Sobhani, H.; Hao, F.; Moshchalkov, V. V.; Dorpe, P. V.; Nordlander, P. Fano Resonances in Individual Coherent Plasmonic Nanocavities. *Nano Lett.* **2009**, *9*, 1663−1667.

(10) Payne, E. K.; Shuford, K. L.; Park, S.; Schatz, G. C.; Mirkin, C. A. Multipole Plasmon Resonances in Gold Nanorods. *J. Phys. Chem. B* **2006**, *110*, 2150−2154.

(11) Zhang, J.; Lakowicz, J. R. Metal-Enhanced Fluorescence of an Organic Fluorophore Using Gold Particles. *Opt. Express* **2007**, *15*, 2598−2606.

(12) Zhang, J. Z.; Noguez, C. Plasmonic Optical Properties and Applications of Metal Nanostructures. *Plasmonics* **2008**, *3*, 127−150.

(13) Kinkhabwala, A.; Yu, Z.; Fan, S.; Avlasevich, Y.; Müllen, K.; Moerner, W. E. Large Single-Molecule Fluorescence Enhancements Produced by a Bowtie Nanoantenna. *Nat. Photonics* **2009**, *3*, 654−657.

(14) Ferry, V. E.; Sweatlock, L. A.; Pacifici, D.; Atwater, H. A. Plasmonic Nanostructure Design for Efficient Light Coupling into Solar Cells. *Nano Lett.* **2008**, *8*, 4391−4397.

(15) Wang, W.; Wu, S.; Reinhardt, K.; Lu, Y.; Chen, S. Broadband Light Absorption Enhancement in Thin-Film Silicon Solar Cells. *Nano Lett.* **2010**, *10*, 2012−2018.

(16) Atwater, H. A.; Polman, A. Plasmonics for Improved Photovoltaic Devices. *Nat. Mater.* **2010**, *9*, 205−213.

(17) Jain, P. K.; Huang, X.; El-Sayed, I. H.; El-Sayed, M. A. Review of Some Interesting Surface Plasmon Resonance-Enhanced Properties of Noble Metal Nanoparticles and Their Applications to Biosystems. *Plasmonics* **2007**, *2*, 107−118.

(18) Skrabalak, S. E.; Chen, J.; Au, L.; Lu, X.; Li, X.; Xia, Y. Gold Nanocages for Biomedical Applications. *Adv. Mater.* **2007**, *19*, 3177−3184.

(19) Kumar, S.; Harrison, N.; Richards-Kortum, R.; Sokolov, K. Plasmonic Nanosensors for Imaging Intracellular Biomarkers in Live Cells. *Nano Lett.* **2007**, *7*, 1338−1343.

(20) Lapotko, D. Therapy with Gold Nanoparticles and Lasers: What Really Kills the Cells? *Nanomedicine* **2009**, *4*, 253−256.

(21) Rodríguez-Oliveros, R.; Sánchez-Gil, J. A. Gold Nanostars as Thermoplasmonic Nanoparticles for Optical Heating. *Opt. Express* **2012**, *20*, 621−626.

(22) Zhang, W.; Huang, L.; Santschi, C.; Martin, O. J. F. Trapping and Sensing 10 nm Metal Nanoparticles Using Plasmonic Dipole Antennas. *Nano Lett.* **2010**, *10*, 1006−1011.

(23) Hrelescu, C.; Sau, T. K.; Rogach, A. L.; Jäckel, F.; Feldmann, J. Single Gold Nanostars Enhance Raman Scattering. *Appl. Phys. Lett.* **2009**, *94*, 153113−153115.

(24) Brian, J. R.; Ko Kaspar, D. K.; Kumar, A.; Fung, K. H.; Chow, E. K. C.; Liu, G. L.; Nicholas, X. F.; Kimani, C.; Toussaint, J. Application of Plasmonic Bowtie Nanoantenna Arrays for Optical Trapping, Stacking, and Sorting. *Nano Lett.* **2012**, *12*, 796−801.

(25) Park, J. -R.; Choi, D. S.; Gracias, D. H.; Leong, T. G.; Presser, N.; Stupian, G. W.; Leung, M. S.; Kim, Y. K. Fabrication and Characterization of RF Nanoantenna on a Nanoliter-Scale 3D Microcontainer. *Nanotechnology* **2011**, *22*, 455303−455307.

(26) Ginzburg, P.; Nevet, A.; Berkovitch, N.; Normatov, A.; Lerman, G. M.; Yanai, A.; Levy, U.; Orenstein, M. Plasmonic Resonance Effects for Tandem Receiving-Transmitting Nanoantennas. *Nano Lett.* **2011**, *11*, 220−224.

(27) Pakizeh, T.; Käll, M. Unidirectional Ultracompact Optical Nanoantennas. *Nano Lett.* **2009**, *9*, 2343−2349.

(28) Kosako, T.; Kadoya, Y.; Hofmann, H. F. Directional Control of Light by a Nano-Optical Yagi-Uda Antenna. *Nat. Photonics* **2010**, *4*, 312−315.

(29) Turkmen, M.; Aksu, S.; Çetin, A. E.; Ali Yanik, A.; Altug, H. Multi-resonant Metamaterials Based on UT-Shaped Nano-aperture Antennas. *Opt. Express* **2011**, *19*, 7921−7928.

(30) Fromm, D. P.; Sundaramurthy, A.; Schuck, P. J.; Kino, G.; Moerner, W. E. Gap-Dependent Optical Coupling of Single "Bowtie" Nanoantennas Resonant in the Visible. *Nano Lett.* **2004**, *4*, 957−961.

(31) Zhang, S.; Genov, D. A.; Wang, Y.; Liu, M.; Zhang, X. Plasmon-Induced Transparency in Metamaterials. *Phys. Rev. Lett.* **2008**, *101*, 047401.

(32) Wustholz, K. L.; Henry, A.-I.; McMahon, J. M.; Freeman, R. G.; Valley, N.; Piotti, M. E.; Natan, M. J.; Schatz, G. C.; Duyne, R. P. V. Structure−Activity Relationships in Gold Nanoparticle Dimers and Trimers for Surface-Enhanced Raman Spectroscopy. *J. Am. Chem. Soc.* **2010**, *132*, 10903−10910.

(33) Hao, E.; Schatz, G. C. Electromagnetic Fields Around Silver Nanoparticles and Dimers. *J. Chem. Phys.* **2004**, *120*, 357−366.

(34) Giannini, V.; Rodriguez-Oliveros, R.; Sánchez-Gil, J. A. Surface Plasmon Resonances of Metallic Nanostars/Nanoflowers for Surface-Enhanced Raman Scattering. *Plasmonics* **2010**, *5*, 99−104.

(35) Rodríguez-Oliveros, R.; Sánchez-Gil, J. A. Localized Surface-Plasmon Resonances on Single and Coupled Nanoparticles Through Surface Integral Equations for Flexible Surfaces. *Opt. Express* **2011**, *19*, 12208−12219.

(36) Aizpurua, J.; Hanarp, P.; Sutherland, D. S.; Käll, M.; Bryant, G. W.; García de Abajo, F. J. Optical Properties of Gold Nanorings. *Phys. Rev. Lett.* **2003**, *90*, 057401.

(37) Petschulat, J.; Cialla, D.; Janunts, N.; Rockstuhl, C.; Hübner, U.; Möller, R.; Schneidewind, H.; Mattheis, R.; Popp, J.; Tünnermann, A.; et al. Doubly Resonant Optical Nanoantenna Arrays for Polarization Resolved Measurements of Surface-Enhanced Raman Scattering. *Opt. Express* **2010**, *18*, 4184−4197.

(38) Tian, C. F.; Ding, C. H.; Liu, S. Y.; Yang, S. C.; Song, X. P.; Ding, B. J.; Li, Z. Y.; Fang, J. X. Nanoparticle Attachment on Silver Corrugated-Wire Nanoantenna for Large Increases of Surface-Enhanced Raman Scattering. *ACS Nano* **2011**, *5*, 9442−9449.

(39) Li, W.-D.; Ding, F.; Hu, J.; Chou, S. Y. Three-Dimensional Cavity Nanoantenna Coupled Plasmonic Nanodots for Ultrahigh and Uniform Surface-Enhanced Raman Scattering over Large Area. *Opt. Express* **2011**, *19*, 3925−3936.

(40) Hatab, N. A.; Hsueh, C. -H.; Gaddis, A. L.; Retterer, S. T.; Li, J. -H.; Eres, G.; Zhang, Z. Y.; Gu, B. H. Free-Standing Optical Gold Bowtie Nanoantenna with Variable Gap Size for Enhanced Raman Spectroscopy. *Nano Lett.* **2010**, *10*, 4952−4955.

(41) Li, H. B.; Xu, S. P.; Liu, Y.; Gu, Y. J.; Xu, W. Q. Directional Emission of Surface-Enhanced Raman Scattering Based on a Planar-Film Plasmonic Antenna. *Thin Solid Films* **2012**, *520*, 6001−6006.

(42) Sarid, D. Long-Range Surface-Plasma Waves on Very Thin Metal Films. *Phys. Rev. Lett.* **1981**, *47*, 1927−1930.
(43) Craig, A. E.; Olson, G. A.; Sarid, D. Experimental Observation of the Long-Range Surface-Plasmon Polariton. *Opt. Lett.* **1983**, *8*, 380−382.
(44) Matsubara, K.; Kawata, S.; Minami, S. Multilayer System for a High-Precision Surface Plasmon Resonance Sensor. *Opt. Lett.* **1990**, *15*, 75−77.
(45) Lyndin, N. M.; Salakhutdinov, I. F.; Sychugov, V. A.; Usievich, B. A.; Pudonin, F. A.; Parriaux, O. Long-Range Surface Plasmons in Asymmetric Layered Metal-Dielectric Structures. *Sens. Actuators B* **1999**, *54*, 37−42.
(46) Toyama, S.; Doumae, N.; Shoji, A.; Ikariyama, Y. Design and Fabrication of a Waveguide-Coupled Prism Device for Surface Plasmon Resonance Sensor. *Sens. Actuators B* **2000**, *65*, 32−34.
(47) Nenninger, G. G.; Tobiska, P.; Homola, J.; Yee, S. S. Long-Range Surface Plasmons for High-Resolution Surface Plasmon Resonance Sensors. *Sens. Actuators B* **2001**, *74*, 145−151.
(48) Liu, Y.; Xu, S. P.; Tang, B.; Wang, Y.; Zhou, J.; Zheng, X. L.; Zhao, B.; Xu, W. Q. Simultaneous Measurement of Surface Plasmon Resonance and Surface-Enhanced Raman Scattering. *Rev. Sci. Instrum.* **2010**, *81*, 036105−036107.
(49) Liu, Y.; Xu, S. P.; Li, H. B.; Jian, X. G.; Xu, W. Q. Localized and Propagating Surface Plasmon Co-enhanced Raman Spectroscopy Based on Evanescent Field Excitation. *Chem. Commun.* **2011**, *47*, 3784−3786.
(50) Jung, H. S.; Kim, K.; Kim, M. S. Raman Spectroscopic Investigation of the Adsorption of 4-Mercaptopyridine on a Silver-Sol Surface. *J. Mol. Struct.* **1997**, *407*, 139−147.
(51) Hu, J. W.; Zhao, B.; Xu, W. Q.; Li, B. F.; Fan, Y. G. Surface-Enhanced Raman Spectroscopy Study on the Structure Changes of 4-Mercaptopyridine Adsorbed on Silver Substrates and Silver Colloids. *Spectrochim. Acta, Part A* **2002**, *58*, 2827−2834.
(52) Liu, Y.; Xu, S. P.; Xuan, X. Y.; Zhao, B.; Xu, W. Q. Long-Range Surface Plasmon Field-Enhanced Raman Scattering Spectroscopy Based on Evanescent Field Excitation. *J. Phys. Chem. Lett.* **2011**, *2*, 2218−2222.
(53) Fang, Y.; Seong, N.; Dlott, D. D. Measurement of the Distribution of Site Enhancements in Surface-Enhanced Raman Scattering. *Science* **2008**, *321*, 388−392.
(54) Lee, P. V.; Meisel, D. Adsorption and Surface-Enhanced Raman of Silver and Gold Sols. *J. Phys. Chem.* **1982**, *86*, 3391−3395.

Supporting Information for Publication

A Long-Range Surface Plasmon Resonance /Probe/ Silver Nanoparticle (LRSPR-P-NP) Nano-antenna Configuration for Surface-Enhanced Raman Scattering

Xuyang Xuan[1], Shuping Xu[1], Yu Liu[2], Haibo Li[1], Weiqing Xu[1], John R. Lombardi[3]*

[1.]State Key Laboratory of Supramolecular Structure and Materials, Jilin University, Changchun 130012, People's Republic of China

[2.]State Key Laboratory of Applied Optics, Changchun Institute of Optics, Fine Mechanics and Physics, Chinese Academy of Sciences, Changchun, Jilin 130033, China

[3.]Department of Chemistry, City College of New York, N.Y. 10031, USA

1. Configuration of the SPR-SERS microspectrometer.

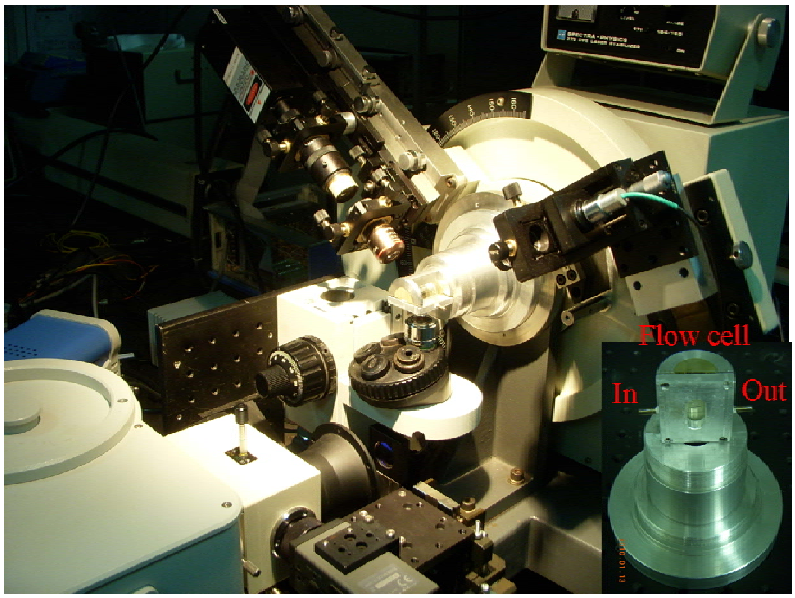

Figure S1. The photo of SPR-SERS microspectrometer and sample platform. The volume of flow cell is 19 mm×9 mm×0.3mm.

Scheme 1 presents a diagrammatic view of how to simultaneously measure the SPR curves and incident angle-dependent SERS spectra by a self-developed SPR-SERS microspectrometer. More details about this instrument and the operation were presented in our previous work.[1] The incident light system was mounted on one arm of a two-arm goniometer, which was comprised of a laser (532 nm, Changchun New Industries Optoelectronics Tech. Co. Ltd), two lenses (Lens 1 has a numerical aperture of 0.18 and a focal length of 25 mm, Lens 2 has a numerical aperture of 0.15 and a focal length of 10 mm) and a polarizer. The laser power was 8 mW for excitation. The LRSPR-P-NP configuration (or a LRSPR configuration) was fixed in the center of the goniometer. The specular reflectance on the prism side and the SERS spectra under the evanescent field were both recorded with the incident angle. The SERS detection system involved an inverted microscope with a 20× objective lens (NA = 0.35, focal length = 20.5 mm),

an edge filter (λ = 532 nm, Semrock Inc.), a focusing lens (Lens 4, focal length = 108 mm) and a spectrometer (iHR320, Jobin-Yvon Co.).

2. The details of FDTD simulation.

The simulation model is shown in Figure 2 (a). Between the silver film and the Ag nanoparticles, there exists a monolayer of 4-Mpy, which plays a role as a linker. 4-Mpy in this structure play a role as linker, they absorbed on the silver film by chemically adsorbed, which could be seen as one monolayer. The diameter of a pyridine ring is about 0.65 nm. The van der Waals radius of the thiol sulfur is about 0.185 nm.[2] So we take the length of 4-Mpy as 1 nm. A nanoparticle laid 1 nm away from a 20 nm-thickness silver film. A p-polarized plane wave propagates above the prism and the incidence angle is set as 64 degree. The wavelength is 532 nm. As the laser irradiation at the interface of the prism and magnesium fluoride, there occurs total reflection because the refractive index suddenly become smaller. This results in the generation of evanescent wave.

The material of film was silver-Palik. The boundary conditions were Bloch in X axis and PML (perfectly matched layer) in Y axis when we simulated the SERS emission on the KR configuration. The refractive index of the prism is 1.52 at 532 nm and the thickness of the silver film is 20 nm. The refractive index of the magnesium fluoride is 1.38 at 532 nm and the thickness of the magnesium fluoride film is 1 μm.

3. Theoretical calculation of the penetration depth.

The penetration depth, d_p, can be expressed in terms of the dielectric constants by $d_p = \frac{\lambda}{2\pi\left(\varepsilon_p \sin^2\theta - \mathrm{Re}\left[\hat{\varepsilon}_D\right]\right)^{1/2}}$. The prism is transparent and has a dielectric constant of ε_P. The dielectric substrate with a semi-infinite thickness has a complex dielectric constant of $\hat{\varepsilon}_D$. An incident beam with the wavelength of λ impinges at the prism/multilayer interface with an incidence angle at θ degree.[3] From the above equation, we calculated the penetration depth, which is 613 nm in a LRSPR structure under present experimental conditions.

4. Assignment of the Raman spectrum of 4-Mpy.

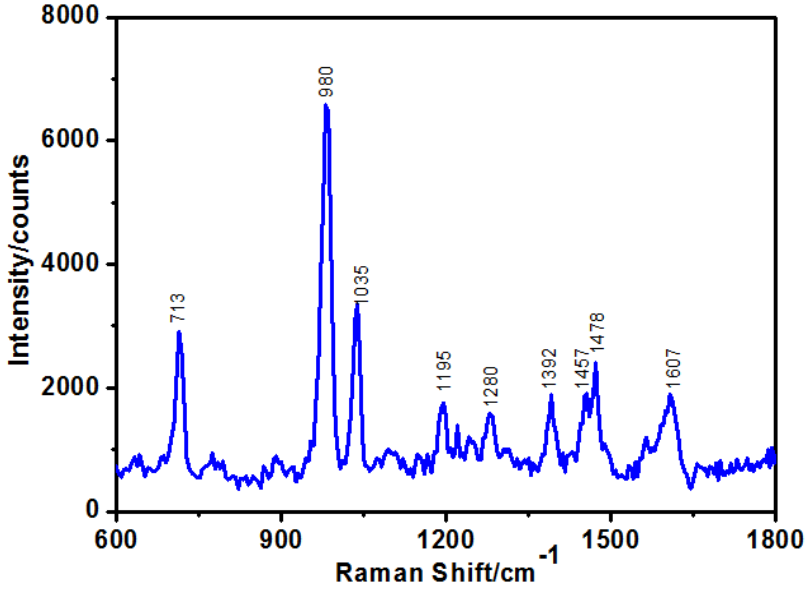

Figure S2. A Raman spectrum of bulk 4-Mpy.

The Raman spectrum of bulk 4-Mpy is shown in figure S2. The band assignments were obtained from Refs [4], [5]. Those at 1392,1457, 1478 and 1607 cm^{-1} are related to the pyridine ring C=C stretching mode, those at 1035, 1195 and 1280 cm^{-1} are associated with the pyridine ring C-H in-plane bending mode, those at 980 and 1100 cm^{-1} arise from the ring breathing modes among which the band at 1100 cm^{-1} is coupled with the C-S stretching, and those below 900 cm^{-1} are mainly due to the pyridine ring deformation and aromatic C-H out-of-plane bending mode.

5. pH sensing.

Here, we applied this LRSPR-P-NP nano-antenna for pH response. Different buffer solutions (citrate acid and Na_2HPO_4 buffers) with different pH values were injected into the flow cell. Figure S3 (A) show the SERS spectrum with the pH value. We plotted Log (A_{1206}/A_{1221}) vs. pH value and found it had a good linear relationship in the pH range of 2-7 (Figure S3 B). The correlation coefficient of the fitted line is 0.9929.

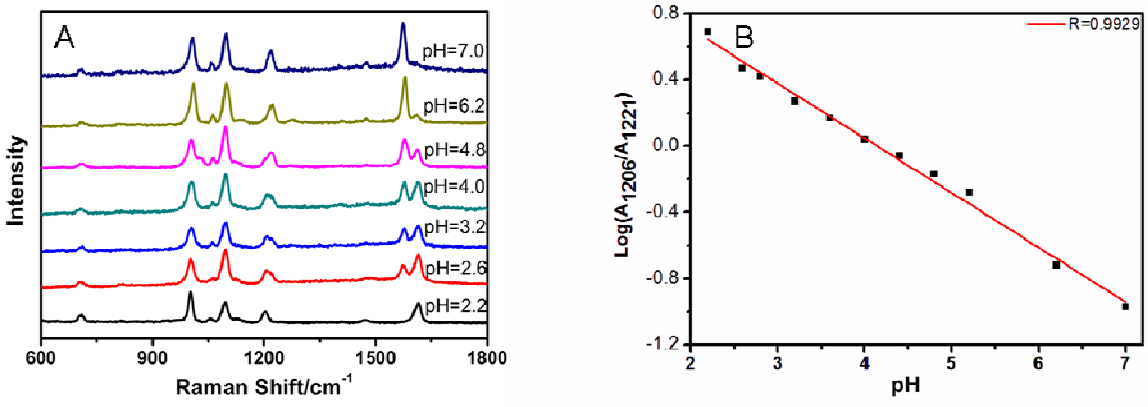

Figure S3 A) The SERS spectra of 4-Mpy with different pH values. The integration time was 1s. B) The working curve of Log (A_{1206}/A_{1221}) vs. pH value.

6. The AFM images of the deposited silver film before and after the assembly of silver NPs.

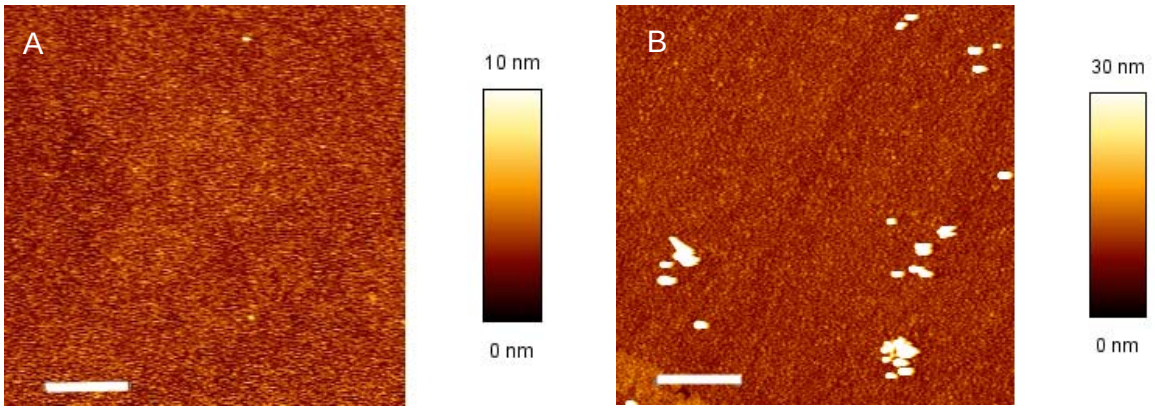

Figure S4 A and B are the AFM images of the flat silver film before and after the assembly of silver nanoparticles. Scale bars are 1μm.

From AFM images we can see that the silver NPs successfully assembled on the surface of the silver film. Although less silver NPs had assembled on the silver film surface, it resulted in a great SERS enhancement (an average enhancement of 40 times).

7. Calculation of the average enhancement factor (G).

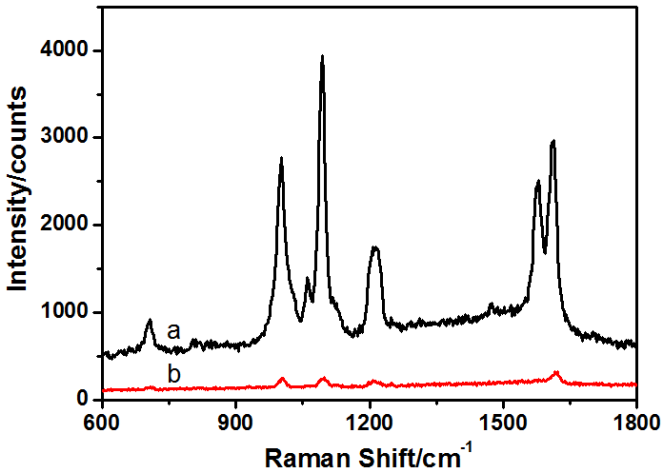

Figure S5. (a) The SERS spectrum of 4-Mpy on the LRSPR-P-NP configuration. The integration time was 1 s. (b) Normal Raman spectrum of 4-Mpy absorbed on a prism. The integration time was 20 s.

Sample for normal Raman measurement were prepared by drop-coating of the 4-Mpy (10 μL, 10^{-3} mol/L) aqueous solution on a normal K9 prism, and then the substrate was dried at room temperature. After the solvent evaporated (2 hours later), the solution formed a circular deposit with a diameter of 4.0 (±0.5) mm.

Samples for SERS measurements were prepared by the sequential drop-coating of the mixed solution of 4-Mpy and classical silver NP [V (4-Mpy, 10^{-7} M): V (silver NPs, 2.5×10^{-11}M) =1:9] aqueous solutions onto the silver film in the LRSPR configuration, and then the substrate was dried in room temperature. After the solvent evaporated (2 hours later), the solution formed a circular deposit with the diameter of 4.2±0.5 mm. The average surface coverage was calculated

to be 4.30×10^{11} molecules/cm^2. Thus, the average occupied area of a 4-Mpy molecule is supposed to be about 2.3×10^{-9} cm^2, which is obviously larger than the maximum surface area per 4-Mpy (about 7.0×10^{-15} cm^2). So, we can infer that the 4-Mpy deposited film was less than a monolayer.

Here, we adopted the estimation of the SERS enhancement factor (G) reported by Gupta and Weimeras. [6]

$$G = \frac{I_{Nano-Antenna} / N_{Nano-Antenna}}{I_{Raman} / N_{Raman}} = \frac{I_{Nano-Antenna}}{N_{Nano-Antenna}} \times \frac{I_{Raman}}{N_{Raman}} \quad \text{..... (1)}$$

Where the $N_{Nano\text{-}Antenna}$ and N_{Raman} denote the number of probe molecules which contribute to the SNP-LRSP SERS signal and normal Raman signals, while the $I_{Nano\text{-}Antenna}$ and I_{Raman} denote the corresponding SERS and normal Raman intensities. In our experiment, because the 4-Mpy adsorbed onto the sliver was a monolayer, the G can be written in the following form,

$$G = \frac{I_{Nano-Antenna}}{A \times \frac{M_{Nano-Antenna}}{S_{Nano-Antenna}}} \times \frac{A \times \frac{M_{Raman}}{S_{Raman}}}{I_{Raman}} = \frac{I_{Nano-Antenna} \times S_{Nano-Antenna} \times M_{Raman}}{I_{Raman} \times S_{Raman} \times M_{Raman}} \quad \text{....} \quad (2)$$

Where the $M_{Nano\text{-}Antenna}$ and M_{Raman} are the number of 4-Mpy molecules dropped onto a sliver film coated prism and a normal prism. The $S_{Nano\text{-}Antenna}$ and S_{Raman} are the geometrical areas of the 4-Mpy film. A is the recorded area of a laser spot. Since SERS spectra were obtained under the same excitation angle, the laser spot area can be ignored. The representative band at 1003 cm^{-1} due to ring-breathing (the band is at 1005 cm^{-1} in the normal Raman spectrum. [7, 8]) was selected to calculate G. The SERS signal intensity at 1003 cm^{-1} is 3346 cps and normal Raman

signal intensity at 1005 cm^{-1} is 6.5 cps (see Figure S5). The $S_{Nano\text{-}Antenna}$ and S_{Raman} are 0.14 and 0.13 cm^2. We calculated G by using the expressions (2) and the value of G is 5.62 ($\pm$0.55) $\times 10^7$.

The repeatability of this nano-antenna for SERS was considered. Table S1 shows the G value for five trials and the standard error is 5.49 %, which indicates this nano-antenna has a good stability and repeatability for SERS measurement.

Table S1 Calculation of the enhancement factor

The number of experiments for enhancement factor					standard error	average value
1	2	3	4	5		
5.609×10^7	5.558×10^7	5.653×10^7	5.567×10^7	5.686×10^7	5.49%	5.615×10^7

References:

(1) Liu, Y.; Xu, S. P.; Tang, B.; Wang, Y.; Zhou, J.; Zheng, X. L.; Zhao, B.; Xu, W. Q. Simultaneous Measurement of Surface Plasmon Resonance and Surface-Enhanced Raman Scattering. *Rev. Sci. Instrum.* **2010**, *81*, 036105–036107.

(2) Wan L.-J.; Noda H.; Hara Y.; Osawa M. Effect of Solution pH on the Structure of a 4-Mercaptopyridine Monolayer Self-Assembled on Au(111). *J. Electroanal. Chem.* **2000**, *489*, 68–75.

(3) Ekgasit S.; Thammacharoen. C.; Knoll. W. Surface Plasmon Resonance Spectroscopy Based on Evanescent Field Treatment. *Anal. Chem.* **2004**, *76*, 561 -568

(4) Jung, H. S.; Kim, K.; Kim, M. S. Raman Spectroscopic Investigation of the Adsorption of 4-Mercaptopyridine on a Silver-sol Surface. *J. Mol. Struct.* **1997**, *407*, 139-147.

(5) Hu, J. W.; Zhao, B.; Xu, W. Q.; Li, B. F.; Fan, Y. G. Surface-Enhanced Raman Spectroscopy Study on the Structure Changes of 4-Mercaptopyridine Adsorbed on Silver Substrates and Silver Colloids. *Spectrochimica Acta Part A* **2002**, *58*, 2827-2834.

(6) Gupta, R.; Weimer, W. A. High Enhancement Factor Gold Films for Surface Enhanced Raman Spectroscopy. *Chem. Phys. Lett.* **2003**, *374*, 302-306.

(7) Baldwin, J. A.; Schühler, N.; Butler, I. S.; Andrews, M. P. Integrated Optics Evanescent Wave Surface Enhanced Raman Scattering (IO-EWSERS) of Mercaptopyridines on a Planar Optical Chemical Bench: Binding of Hydrogen and Copper Ion. *Langmuir* **1996**, *12*, 6389-6398.

(8) Baldwin, J. A.; Vlckova, B. M.; Andrews, P.; Butler, I. S. Surface-Enhanced Raman Scattering of Mercaptopyridines and Pyrazinamide Incorporated in Silver Colloid-Adsorbate Films. *Langmuir* **1997**, *13*, 3744-3751.